Research Article Vol. 62, No. 10 / 1 April 2023 / Applied Optics 2479

applied optics

Chatter-suppressing ruling method based on double-layer elastic support

Shuo Yu, Jirigalantu,* Hongzhu Yu, Xuefeng Yao, and Wenhao Li

Changchun Institute of Optics, Fine Mechanics and Physics, Chinese Academy of Sciences, Changchun, 130033, China
**jiri5998@163.com*

Received 2 January 2023; revised 12 February 2023; accepted 13 February 2023; posted 15 February 2023; published 21 March 2023

A cross-hinge spring is the preferred support for a ruling tool because of its excellent flexibility. However, there are high precision requirements for the tool installation, which make the installation and adjustments difficult. There also is poor robustness against interference, which readily results in tool chatter. These issues affect the quality of the grating. This paper proposes an elastic ruling tool carrier with a double-layer parallel-spring mechanism, establishes a torque model of the spring, and analyzes its force state. In a simulation, the spring deformation and frequency modes of the two ruling tool carriers are compared and the overhang length of the parallel-spring mechanism is optimized. In addition, the performance of the optimized ruling tool carrier is analyzed in a grating ruling experiment to verify the carrier's effectiveness. The results show that compared to the cross-hinge elastic support, the deformation of the parallel-spring mechanism by a ruling force in the *X* direction is on the same order of magnitude. However, the deformation in the *Y* direction is reduced by a factor of 270, and the deformation in the *Z* direction is reduced by a factor of 32. The torque of the proposed tool carrier is slightly higher (12.8%) in the *Z* direction but lower by a factor of 2.5 in the *X* direction and by a factor of 60 in the *Y* direction. The overall stiffness of the proposed tool carrier is improved and the first-order frequency of the proposed structure is higher by a factor of 2.8. The proposed tool carrier thus better suppresses chatter, effectively reducing the effect of the ruling tool installation error on the grating quality. The flutter suppression ruling method can provide a technical basis for further research on high-precision grating ruling manufacturing technology.

https://doi.org/10.1364/AO.484486

1. INTRODUCTION

Gratings are widely used in astronomy, medical treatment, precision displacement measurement and other fields, and they are the core device in many precision instruments [1–4]. Some types of grating masters, such as echelle masters, are mostly prepared through mechanical ruling [5]; i.e., a diamond chisel-edge tool installed on a tool carrier is driven with reciprocating motion in the direction of the grating line by the guide rail of the ruling machine, and the substrate moves unidirectionally in the grating periodic direction, as shown in Fig. 1. Ruling a large area echelle often requires ruling tools to continuously ruling more than 10 kilometers. This process is different from the general cutting process because it does not produce chips but relies on the "ploughing" extrusion effect, resulting in a periodic groove shape on aluminum film. This extrusion process has strict requirements for the installation angle of the tool [6–8]. Until now, the Changchun Institute of Optics, Fine Mechanics and Physics at the Chinese Academy of Sciences successfully developed large-scale grating mechanical ruling equipment and produced echelles with the largest area achieved worldwide [9,10]. Although research of the ruling equipment is nearly complete, to the best of our knowledge, the elastic ruling tool carrier that is closely connected with the ruling tool has yet not been systematically studied. When there is a certain precision error in the installation of the ruling tool, its elastic structure will lead to the occurrence of chatter. This chatter will make the depth and shape of the groove deviate from the ideal grating groove shape and can even affect the service life of the ruling tool. It is therefore difficult to adjust the installation angle of the ruling tool and is not conducive to maintain the stability of the ruling system in a large ruling distance.

The chatter in machining relates to self-vibration and can be classified based on its generation mechanism as regenerative chatter, compound chatter, and friction chatter [11–13]. No matter what the cause, the suppression of chatter can be classified as two types: initiative suppression, where the driver affects the control target through the monitored chatter signal [14], and passive suppression, as adopted in this paper, where the process parameters or machine and ruling tool stiffness are improved. Jin *et al*., for example, studied the effects of changes in the spindle speed and milling cutter structural parameters on chatter during milling and concluded that a linear change in the milling cutter pitch and a sinusoidal disturbance of the spindle speed can effectively suppress chatter [15]. Li *et al*. analyzed different turning parameters by establishing a model to predict

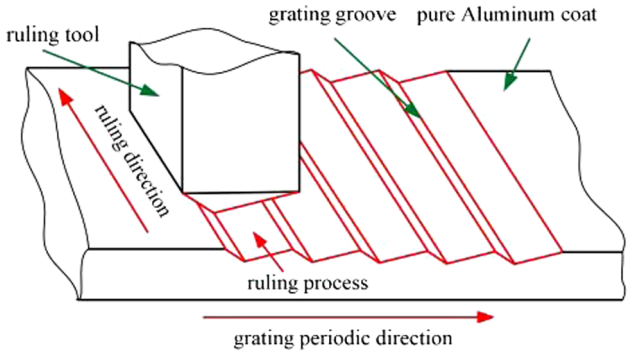

Fig. 1. Schematic diagram of the grating ruling process.

the turning temperature and include vibration signals measured by an acceleration sensor and found that the cutting depth was the primary factor affecting the turning vibration [16]. Ma designed a milling tool with double damping blocks inside the toolbar, and the dynamic damping characteristics increased the chatter suppression [17]. Shi *et al*. identified the chatter during the ruling process from the energy aspect through the force signal sensor and obtained the critical ruling speed according to the experimental results. Therefore, the chatter can be reduced by limiting the ruling speed, but this approach is obviously not suitable for a large-sized echelle ruling process with several weeks of ruling time [18]. The current research on chatter suppression is focused on the high-speed chip removal machining such as milling and cutting. There is no discussion on the chatter about the low-speed extrusion ruling mode. By analyzing the chatter suppression methods of these scholars, the optimization of the stiffness of the mechanism itself is the best means to suppress grating ruling chatter.

Previous studies have optimized the guide angles of the ruling tool and balanced the moments in the ruling process [19]. The chatter phenomenon is suppressed from the perspective of the tool's ruling state. However, there is still chatter when the tool is installed at an imprecise deflection angle, defined as the deflection of the tool edge in the horizontal direction, as shown in Fig. 2. It is the observation image of the grating aluminum film blank under a low-power microscope when ruling tool chatter occurs. There are obvious periodic light and dark stripes in the figure, and the zero-order surface of the grating is deformed to varying degrees, which is precisely the change of the groove ruling state caused by the tool's periodic chatter. This situation will

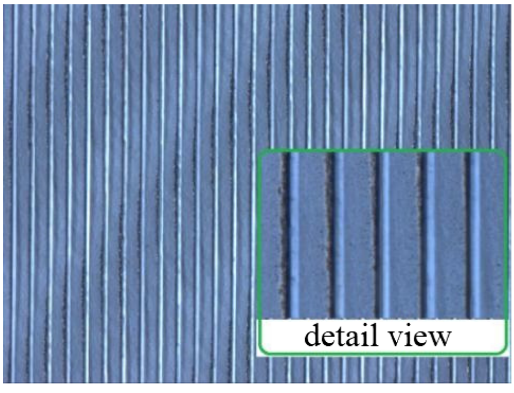

Fig. 2. Ruling chatter phenomenon with a deviation in the deflection angle.

lead to large stray light and ghost lines. Therefore, the best way to solve this kind of problem is to optimize the elastic structure of the ruling tool carrier, which is the source of the chatter. The stability of grating manufacturing can be further improved, and it will be easier to obtain a high-quality grating.

2. OPTIMIZATION AND MECHANICAL ANALYSIS OF THE ELASTIC SUPPORT MECHANISM OF THE RULING TOOL

The elastic support part of the ruling tool carrier uses a cross flexible hinge mechanism. Compared to the general hinge mechanism, there is no friction or clearance. The mechanism relies on the elastic deformation of a spring to realize the lift and fall movements of the ruling tool. The mechanism has a high repetition accuracy and is suitable for the periodic ruling of a grating. The structure, as shown in Fig. 3, has two main parts: the main ruling tool carrier area and the auxiliary ruling tool carrier area. The former connects with the guide rail of the grating ruling machine, and the latter realizes the lifting and falling of the tool and can be used to adjust the installation angle of the tool. These two areas are fixed and connected with the spring by pressing the gasket with eight sets of 16 screws and provide a flexible buffer for the ruling process to prevent tool damage.

The initial design of the flexible hinge reduces the influence of the spray point on the ruling tool edge caused by the low material purity coating on the grating substrate. These spray points are like sand in a sponge, which will cause the edge to crack. Hard contact can be avoided by using the flexible rise and fall of the tool carrier. However, this cross-spring mechanism itself is subject to the phenomena of a center shift and warping, as shown in Fig. 4. A center shift is the phenomenon that the ideal rotation center drifts with an increase in the rotation angle, which affects the axial stability and anti-interference ability of the mechanism. Warping is a phenomenon that happens when the spring is staggered in the direction of the rotation central axis (the Z axis in Fig. 4). There are pairs of reaction forces of the spring P1" and P2" with opposing directions on different sections of the axis, which resulting in the spring twisting around the X axis, and the hinge thus deforms in the nonfunctional direction [20,21]. The two phenomena induce the dynamic imbalance of the ruling force and cause chatter as an excitation source.

To fundamentally solve the phenomenon above, it is necessary to change the connection form of the flexible hinge mechanism. Therefore, a new form of double-layer parallel-spring mechanism is proposed, as shown in Fig. 5. In this connection mode, the two springs are no longer staggered,

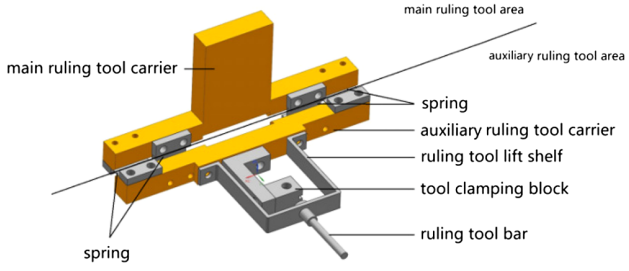

Fig. 3. Grating ruling tool carrier with a cross flexible hinge.

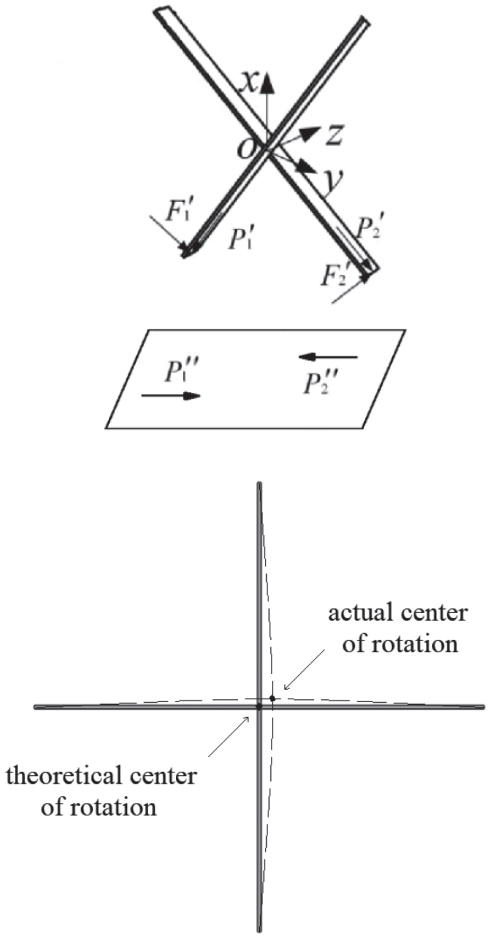

Fig. 4. Phenomena of the center shift and warping of the cross-spring mechanism.

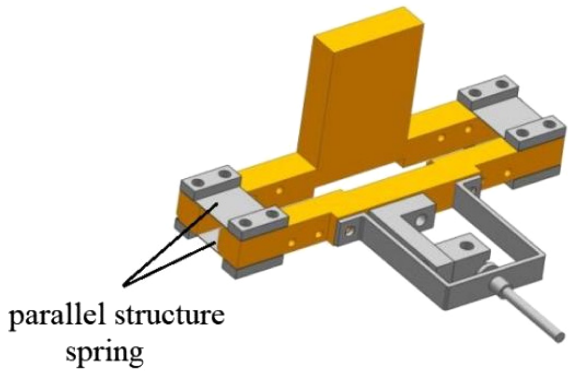

Fig. 5. Grating ruling tool carrier with a parallel-spring mechanism.

the rotation centers are no longer crossed and overlapped, but become parallel, eliminating the center shift and warping during the rotation of the cross hinge, and eight sets of 16 screws are also used for fixation. Although the rotation range of the spring is reduced, the elasticity still provides the protection function of the ruling tool edge and the dynamic adjustment function in the ruling process.

From the perspective of theoretical analysis, the main ruling tool carrier part is fixed during ruling and is thus regarded as a rigid body. Each spring in the tool carrier system can be equivalent to the classical fixed simply supported beam shown in Fig. 6. Based on this state, the deformation in each direction of the spring under the action of the ruling force during the ruling process is analyzed. According to the Euler–Bernoulli beam theory, the curvature at any point on the neutral axis of the beam is the direct ratio to the external force moment acting on the section:

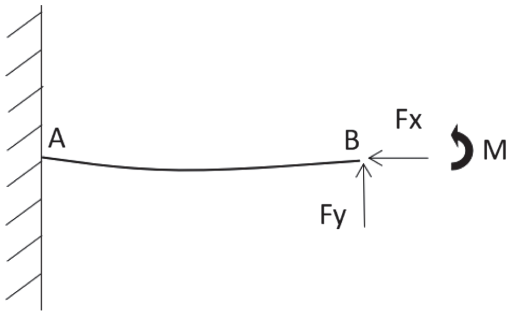

Fig. 6. Equivalent mechanical analysis model of the carrier single spring.

$$M = EI(s)\frac{d\theta}{ds}, \tag{1}$$

where M is the external torque, E is the elastic modulus of the spring, s is the length between the given point and the fixed end of the spring leaf along the neutral axis, $\frac{d\theta}{ds}$ is the curvature of the neutral axis of the section, and $I(s)$ is the moment of inertia of the section.

There is no difference between the cross-spring ruling tool carrier and the parallel-spring ruling tool carrier except for the spring arrangement. Thus, there is no difference in the load acting in each direction. On this basis, force analysis models of the cross-spring ruling tool carrier and parallel-spring ruling tool carrier were established, as shown in Fig. 7. In the figure, F_r is the ruling force acting on the ruling tool carrier, which has the components F_{rx}, F_{ry}, and F_{rz}.

At the fixed point A1 of the cross-spring mechanism,

$$M_1 = F_{rx} \times z_1, \tag{2}$$

$$M_2 = F_{rx} \times y_2, \tag{3}$$

$$M_3 = F_{ry} \times z_1, \tag{4}$$

$$M_4 = F_{rz} \times y_2. \tag{5}$$

At fixed point $A1'$ of the double-layer parallel-spring mechanism,

$$M_5 = F_{rx} \times z_{1'}, \tag{6}$$

$$M_6 = F_{ry} \times z_{1'}, \tag{7}$$

$$M_7 = F_{rx} \times y_{2''}, \tag{8}$$

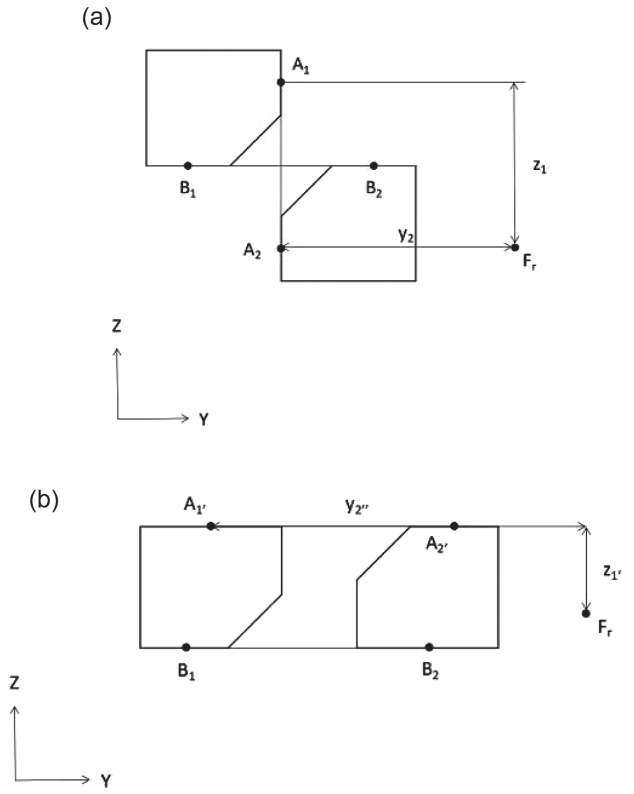

Fig. 7. Force analysis models of ruling tool carriers in the ruling state: (a) ruling tool carrier with a cross-spring mechanism and (b) ruling tool carrier with a parallel-spring mechanism.

$$M_8 = F_{rz} \times y_{2''}. \tag{9}$$

The analysis of the moment in the X direction is omitted because there is no difference in the ruling force Fr in the X direction between the two carrier support points. M_3, M_4, M_6, and M_8 are the moments that twist the carrier around the X axis, M_1 and M_5 are the moments that twist the carrier around the Y axis, and M_2 and M_7 are the moments that twist the carrier around the Z axis.

A comparison of Eqs. (4) and (5) and Eqs. (7) and (9) reveals that the moment along the X axis is more complex, which relates to the magnitude of the ruling force in all directions and the structural parameters of the carrier. For the moment along the Y axis, Eqs. (2) and (6) show that $z_{1'} < z_1$, which means that the parallel-spring mechanism performs better than the cross-spring mechanism in this direction. For the moment along the Z axis, the comparison between Eqs. (3) and (8) shows that $y_2 < y_{2''}$, which means that the cross-spring mechanism performs better than the parallel-spring mechanism in this direction.

3. MECHANICAL SIMULATION OF THE ELASTIC SUPPORT MECHANISM OF THE RULING TOOL

To explore the deformation and stress of the tool carriers during the ruling process, and further compare the ruling state of the two tool carriers, finite element simulation analysis is carried out. Previous grating ruling experience has shown that the ruling force of the grating ruling tool in different directions is on the order of $10 \times e^{-2}$ N, and the three ruling forces $F_x = 0.03$ N, $F_y = 0.04$ N, and $F_z = 0.05$ N are thus applied to the clamping block in the present simulation. Here, the X direction is the direction of the rotation axis of the cross-spring mechanism, the Y direction is the direction orthogonal to the X direction on the horizontal plane, and the Z is the vertical direction. Its maximum overall dimensions are 72 mm × 60 mm × 37 mm. The fixed support constraint is loaded on the main ruling tool area. At the same time, the spring plate is set to 65 Mn, its Poisson's ratio is 0.288, its elastic modulus is 1.97×10^5 MPa, and the density is 7.81 g/cm^3. Some materials of the main and auxiliary tool carriers are set as structural steel, Poisson's ratio is 0.3, the elastic modulus is 2×10^5 MPa, and the density is 7.85 g/cm^3. After grid division, the number of cross-spring mechanism elements is 100601, the number of grid nodes is 201982, the number of double-layer parallel spring mechanisms is 102246, and the number of grid nodes is 209393. The final simulation results are shown in Fig. 8. The displacement of the double-layer spring under the action of the ruling force is a vertical translation of the overall auxiliary ruling tool carrier area, whereas that of the cross-spring mechanism is an overturning movement along the rotation axis of the flexible hinge, which will affect the tool pitch angle and more likely reduce the stability in the ruling process. When the spring deformations of the two carriers are of the same order of magnitude, the deformations at the end of the carriers differ by a factor of 32. The maximum deformation of the cross-spring tool carrier is 7.61×10^{-2} mm, and the maximum deformation of the parallel-spring tool carrier is 2.37×10^{-3} mm. This shows that the parallel-spring ruling tool carrier provides a flexible mechanism equivalent to that of the cross-spring ruling tool carrier and reduces the displacement of each part at the same time. In terms of the grating ruling process, the overturning of the tool carrier not only affects the depth of the tool ruling into the aluminum film on the grating substrate, but also changes the original installation angle between the tool and the aluminum film on the grating substrate, which is more likely to damage the stability of the ruling process and make it difficult for the ruling system to recover to the equilibrium state.

The relationship between the ruling force and displacement in each direction of the two ruling tool carriers is extracted, as shown in Fig. 9. The maximum deformation of the auxiliary ruling tool carrier area in each direction is given in Table 1. Note that the carrier deformation of the two structures increases linearly with the ruling force; the new structure does not change the mapping relationship between the ruling force and the deformation of the hinge mechanism. Compared to the cross-spring ruling tool carrier, the deformation of the parallel-spring ruling tool carrier in the X direction is slightly greater when subjected to the ruling force, but on the same order of magnitude. Comparing the parallel-spring mechanism to the cross-spring mechanism shows that the deformation in the Y direction is reduced by a factor of 270 and the deformation in the Z direction is reduced by a factor of 32. Additionally, the parallel-spring mechanism has much better overall stiffness. After connecting the main and auxiliary tool carrier through the parallel-spring structure, the stability of the tool carrier in the ruling process is increased, and the deformation under the ruling forces is reduced.

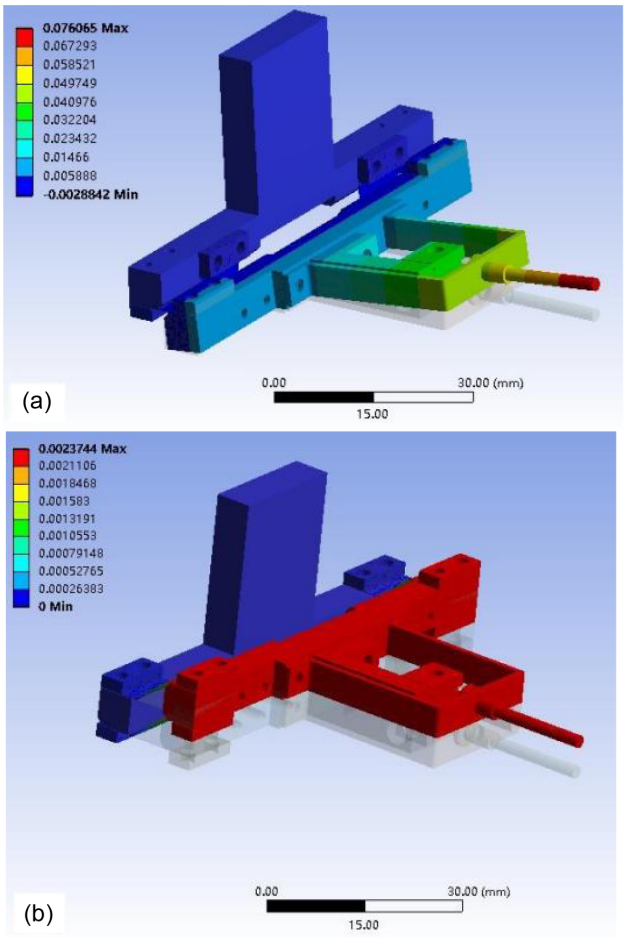

Fig. 8. Strain nephograms of two ruling tool carriers under the effect of the ruling force: (a) cross-spring mechanism and (b) parallel-spring mechanism.

Table 1. Maximum Displacement in Three Directions

	X	*Y*	*Z*
Cross spring	$2.29 \times e^{-5}$	$8.52 \times e^{-3}$	$7.61 \times e^{-2}$
Parallel spring	$2.73 \times e^{-5}$	$3.15 \times e^{-5}$	$2.37 \times e^{-3}$

Similarly, the torque in all directions of the ruling tool carrier under the action of the ruling force is analyzed, as shown in Fig. 10. It is seen that the torque in each direction of the spring increases linearly with the ruling force. The torque in the *Z* direction is slightly higher (12.8%) for the parallel-spring mechanism than for the cross-spring mechanism. However, in the *X* direction it is lower by a factor of 2.5 and in the *Y* direction it is lower by a factor of 60, which is consistent with the law for the simplification of a simply supported beam; therefore, the correctness of the theoretical model in Fig. 7 is verified. This once again confirms that the mechanical properties and deformation of the parallel-spring mechanism when subjected to a force are suitable for the ruling process, and the carrier system thus disturbs the ruling system less.

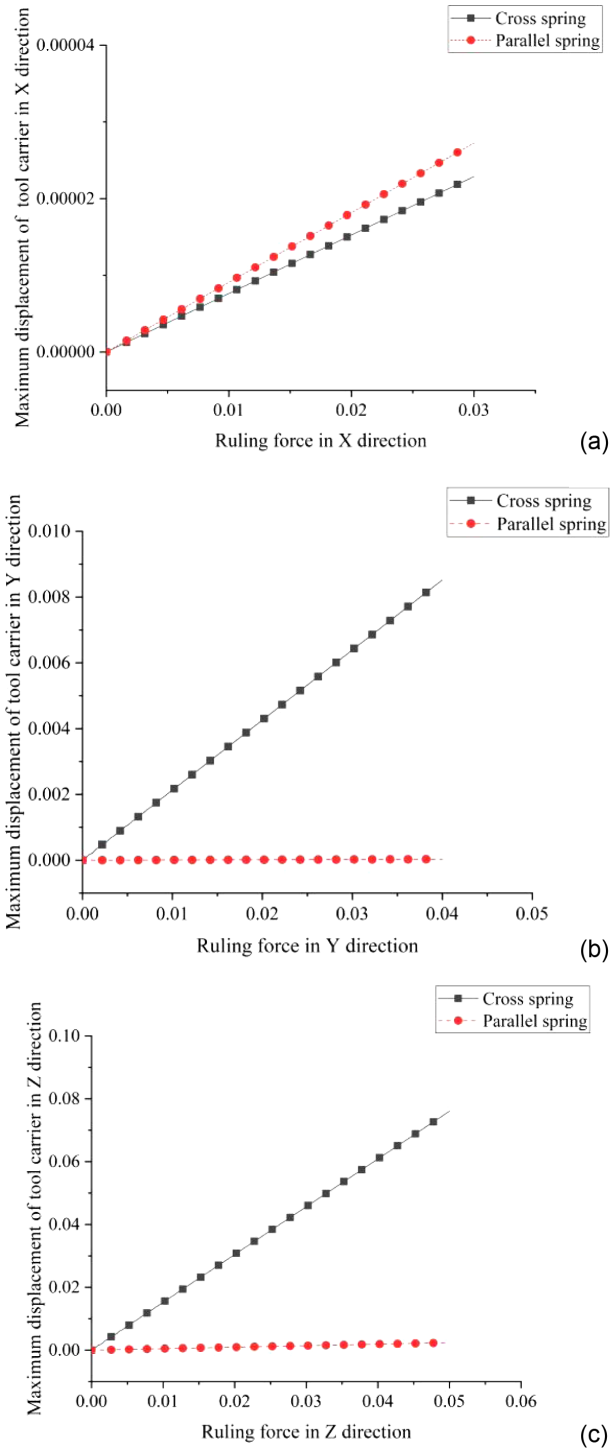

Fig. 9. Effect of the 3D ruling force on the deformation of the two ruling tool carriers: (a) *X* direction, (b) *Y* direction and (c) *Z* direction.

4. MODAL ANALYSIS OF THE ELASTIC SUPPORT MECHANISM OF THE RULING TOOL

Altintas and Aleck found that the frequency of the excitation source that causes chatter is close to the natural frequency of the processing system [22]. It is thus necessary to analyze the modes of the two carriers to further explore the stiffness difference. The first four natural frequencies of the two carriers obtained in a simulation are given in Table 2.

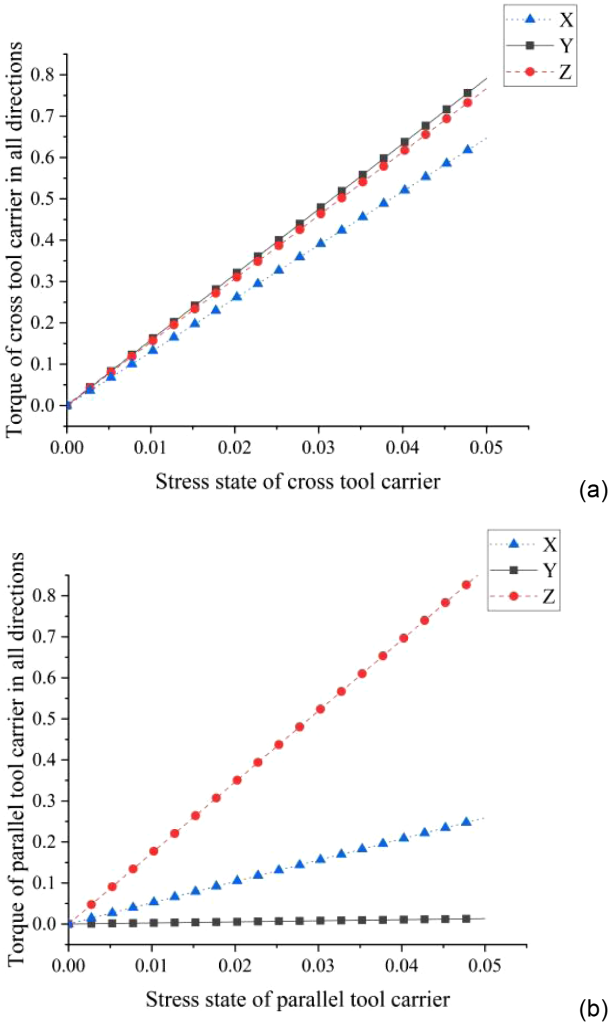

Fig. 10. Torque comparison of the two ruling tool carriers under a ruling force: (a) cross-spring mechanism and (b) parallel-spring mechanism.

Table 2. First Four Natural Frequencies of the Two Ruling Tool Carriers

Model	First Order Frequency	Second Order Frequency	Third Order Frequency	Fourth Order Frequency
Cross spring	80.9	1071.9	2299.8	2642
Parallel spring	224.5	981.8	1067	1568.7

Table 2 shows that the first-order natural frequency of the parallel-spring mechanism is higher than that of the cross-spring mechanism by a factor of 2.8, which once again shows that the stiffness of the new mechanism is much higher than that of the cross-spring mechanism. The first-order natural frequency of the parallel-spring mechanism is far from the frequency of the excitation source in environment. Although the higher-order frequencies of the parallel-spring mechanism are lower than those of the cross-spring mechanism, they are on the order of 1000 Hz and do not readily generate chatter. The parallel-spring mechanism is thus more stable under external excitation and can avoid a drastic change in the ruling force.

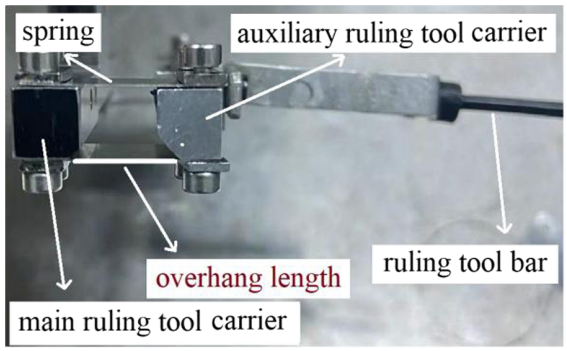

Fig. 11. Overhang length of the parallel-spring mechanism.

Table 3. First Three Natural Frequencies for Different Overhang Lengths

Spring Length (mm)	Overhang Length (mm)	First Order Frequency	Second Order Frequency	Third Order Frequency
14	3	655.33	1076.1	1396.6
16	5	346.45	1067.8	1070.3
18	7	224.56	981.8	1067.2

For the parallel-spring ruling tool carrier, the difference in the overhang length between the main ruling tool carrier and auxiliary ruling tool carrier affects the stiffness, as shown in Fig. 11. The carrier modes are analyzed for different overhang lengths to explore the effect. Table 3 gives the simulation results of the first three natural frequencies.

Table 3 shows that all modes tend to increase with a reduction in the overhang length of the spring. However, the design of the carrier cannot blindly pursue high modes and high stiffness. It must also consider the flexibility of the flexible hinge. An overhang of 7 mm is selected for the parallel-spring ruling tool carrier to balance the required flexibility and stiffness.

5. GRATING RULING EXPERIMENTS UNDER DIFFERENT RULING TOOL CARRIERS

To verify the suppression effect of the new parallel-spring tool carrier on chatter in ruling process when there is an error in the tool azimuth, a 100 gr/mm echelle ruling contrast experiment was conducted with two tool carriers. The experiment was carried out using the CIOMP-5 ruling machine from the Changchun Institute of Optics, Fine Mechanics and Physics at the Chinese Academy of Sciences at an ambient temperature of 21°. The ambient temperature can be controlled to ±0.02°. The selected ruling tool is used to machine echelle with a large blaze angle, and the orientation angle is about 64°. First, the original tool carrier was used to adjust the installation angle of the tool. After the straight groove and regular groove gratings can be engraved, other parameters except the azimuth angle were kept unchanged. The azimuth angle was continuously adjusted for trial ruling until a slight chatter phenomenon was observed. The grating groove with slight chatter was taken as the first observation target. After recording the azimuth parameters,

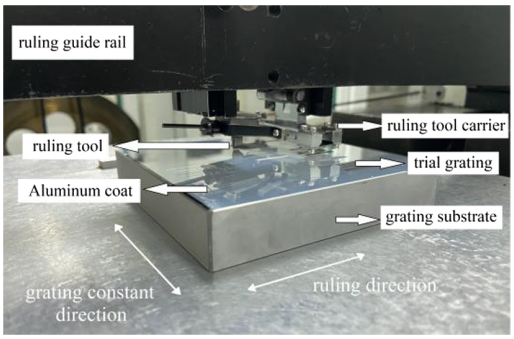

Fig. 12. Grating ruling experiments conducted with the CIOMP-5.

this ruling tool was replaced by the new tool carrier, which was adjusted to the recorded installation angle, and this ruling grating was designated as the second observation target. Finally, the ruling effects of the two tool carriers under the same process parameters were compared. The ruling experiment setup is shown in Fig. 12.

The results of the grating ruling using the two ruling tool carriers were observed under a microscope, as shown in Figs. 13 and 14. Figure 13 shows the results under a 20× objective lens whereas Fig. 14 shows the results under a 50× objective lens. The figures show that when the deflection angle was deflected by a certain angle, chattering occurred for the cross-spring ruling tool carrier, just like in Fig. 2. Obvious light and dark stripes were seen under the low-power objective lens; due to the small deflection angle, the phenomenon of light–dark alternation is relatively light, which is also a common phenomenon in ruling. Under the high-power objective lens, there was more obvious bending of the groove zero-order surface, and the grating surface had periodic deformation, which would greatly affect the working state of the grating and introduce stray light. However, these phenomena were not observed for the proposed tool carrier with the same tool installation parameters under either the low-power or the high-power objective lens; the grating ruling lines appeared straight and regular. The phenomena above verify the conclusion obtained in a previous paper; that is, the new elastic support structure of double-layer tool carrier can reduce the chatter phenomenon caused by the tool deflection installation error to a certain extent.

6. CONCLUSION

This paper proposed a double-layer, parallel-spring ruling tool carrier, which suppresses the shaft drift and warping of the original cross-spring ruling tool carrier, to solve the problem of chatter generated by the deviation of the ruling tool edge in the existing grating ruling process. When a torque mechanical model of the spring ruling was established, it was found that the torque of the proposed carrier was lower in the X direction (i.e., the carrier rotation axis) and the Y direction (i.e., the direction horizontally orthogonal to the carrier rotation axis). The disturbance to the carrier system during ruling was thus reduced. This result was verified in a finite element analysis. The torque of the proposed carrier in the X direction was lower by a factor of 2.5 and the torque in the Y direction was lower by a factor of 60 compared to the torques of the cross-spring ruling tool carrier.

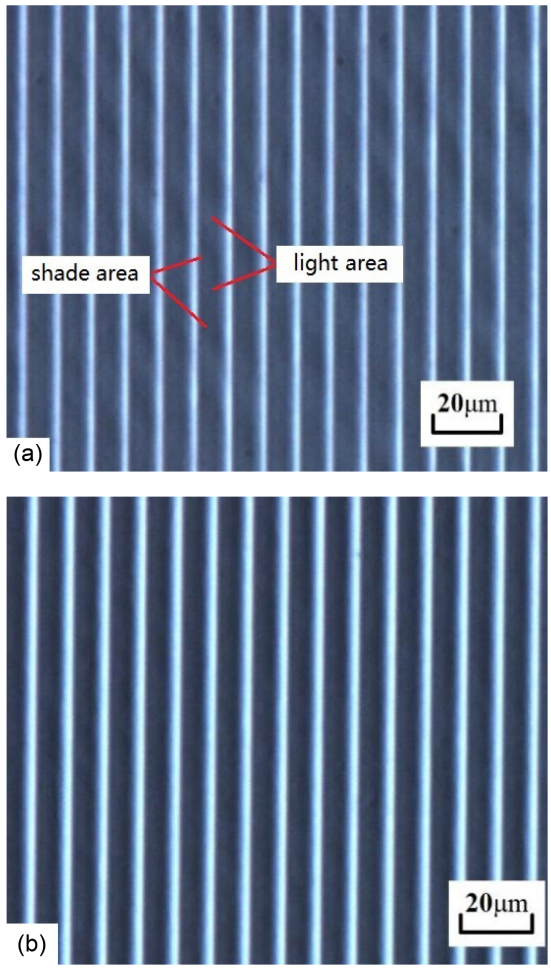

Fig. 13. Grating images under a low-power objective lens: (a) original cross-spring ruling tool carrier and (b) optimized ruling tool carrier.

The simulation results showed that the deformation of the proposed ruling tool carrier structure in the X direction is equivalent to that of the cross-spring tool under the action of a ruling force, but the deformation in the Y direction is lower by a factor of 270, and the deformation in the Z direction is lower by a factor of 32. Additionally, the deformation mode is not an overturning rotation but rather a vertical translation, which suppresses the effect on the tool installation angles in the ruling process and increases the system stability. At the same time, the first-order natural frequency of the proposed carrier is higher by a factor of 2.8 and far from the frequency of the general excitation source, reducing the probability of chatter. Modal analysis for different overhang lengths of the spring and the actual hardness of the ruling tool carrier was carried out to further optimize the double-layer parallel-spring mechanism, and the final overhang length was 7 mm.

The grating ruling experiment showed that for the same deflection angle and other process parameters, the optimized ruling tool carrier obviously inhibited chatter, the grating ruling line was straighter, and the grating surface was more regular. Therefore, the new tool carrier can be used in the mechanical ruling process of gratings to suppress chatter generated by

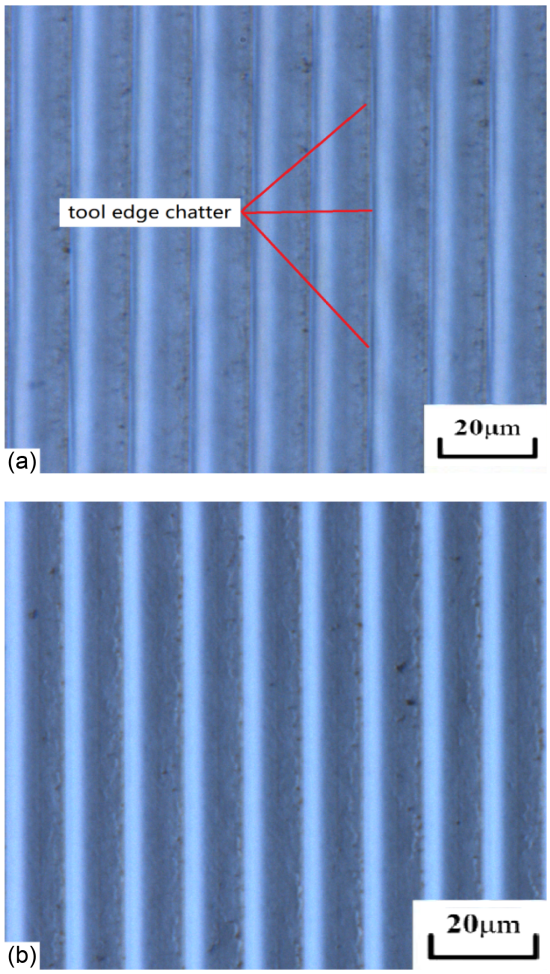

Fig. 14. Grating images under a high-power objective lens: (a) original cross-spring ruling tool carrier and (b) optimized ruling tool carrier.

deflection angle errors. The proposed ruling system hardly experiences instability and chatter when encountering occasional external disturbances in the process of large-area, long-range ruling and is thus very useful for practical applications in the grating manufacturing field. The tool carrier optimization results and the method of chatter suppression can provide the process and technical basis for further research on high-precision grating ruling technology.

Funding. National Natural Science Foundation of China (62075216).

Acknowledgment. Author Jirigalantu thanks the National Natural Science Foundation of China for help identifying collaborators for this work.

Disclosures. The authors declare no conflicts of interest.

Data availability. Data underlying the results presented in this paper are not publicly available at this time but may be obtained from the authors upon reasonable request.

REFERENCES

1. T. Andrea, D. Johannes, T. Simon, G. Harald, and H. Alois, "3D-printed miniature spectrometer for the visible range with a 100 × 100 μm^2 footprint," Light Adv. Manuf. **2**, 20–30 (2021).
2. Y. F. Yin, Z. W. Liu, S. Jiang, W. Wang, H. Z. Yu, W. H. Li, and Jirigalantu, "Grating-based 2D displacement measurement with quadruple optical subdivision of single incident beam," Opt. Express **29**, 24169–24181 (2021).
3. S. Prithiviraj, L. Alyson, T. Avery, and F. Konstantinos, "Variable shearing holography with applications to phase imaging and metrology," Light Adv. Manuf. **3**, 1–18 (2022).
4. N. Kazanskiy, N. Ivliev, V. Podlipnov, and R. Skidanov, "An airborne Offner imaging hyperspectrometer with radially-fastened primary elements," Sensors **20**, 3411 (2020).
5. J. S. Wang, Bayanheshig, and C. A. Zhu, "Dual-drive long-travel precise positioning stage of grating ruling engine," Int. J. Adv. Manuf. Technol. **93**, 3541–3550 (2017).
6. X. T. Mi, S. W. Zhang, H. Z. Yu, H. L. Yu, M. Cong, and X. D. Qi, "Using a unique mirror to minimize the effect of ruling engine cosine error on grating performance," Appl. Opt. **57**, 10146–10151 (2018).
7. Jirigalantu, X. T. Li, X. T. Mi, K. Liu, and Y. G. Tang, "Development of a parameterized mechanical model of a chisel-edge grating ruling tool," Precis. Eng. **50**, 388–392 (2017).
8. B. Q. Zhang, S. Yu, Jirigalantu, Y. J. Wei, and Z. Pang, "Effect of the number of aluminum film layers on the grating ruling plastic grooving process," J. Plast. Eng. **28**, 141–147 (2021).
9. X. F. Yao, J. C. Cui, H. L. Yu, X. D. Qi, X. T. Mi, Y. M. Jiang, M. J. Wang, and X. T. Li, "An improved accuracy-measuring method in manufacturing the lead screw of grating ruling engine," Precis. Eng. **27**, 344–353 (2013).
10. Y. G. Tang, Bayanheshig, C. A. Zhu, and Y. Jin, "Uncover the king of precision machinery," Chin. Basic Sci. **20**, 48–52 (2018).
11. K. Yang and L. X. Huang, "Review of chatter issues in machining," Chin. J. Appl. Mech. **36**, 1464–1470 (2019).
12. Y. V. Petrakov, "Chatter suppression technologies for metal cutting," Mech. Adv. Technol. **2**, 51–58 (2019).
13. Z. X. Wang, X. L. Liu, M. Y. Li, S. Y. Liang, L. H. Wang, Y. Q. Li, and B. Y. Meng, "Intelligent monitoring and control technology of cutting chatter," J. Mech. Eng. **56**, 1–23 (2020).
14. S. Sarath and P. S. Paul, "Application of smart fluid to control vibration in metal cutting: a review," World J. Eng. **18**, 458–479 (2021).
15. G. Jin, H. J. Qi, Z. J. Li, and J. X. Han, "Dynamic modeling and stability analysis for the combined milling system with variable pitch cutter and spindle speed variation," Commun. Nonlinear Sci. Numer. Simul. **63**, 38–56 (2018).
16. D. Q. Li, S. C. Li, Y. T. Hu, and Z. Y. Chen, "Research on the relationship between turning temperature rising and turning vibration based on particle swarm optimization," Trans. Can. Soc. Mech. Eng. **45**, 273–286 (2020).
17. Y. Ma, "Basic research on dynamic characteristics of damping and dynamic anti-vibration cutter based on chatter suppression mechanism," (Jiangsu University, 2020).
18. G. F. Shi, Y. Y. Lv, G. Q. Shi, Jirigalantu, and W. Xiao, "Mechanism of frictional chatter during mechanical ruling grating," Opt. Precis. Eng. **22**, 3061–3066 (2014).
19. Jirigalantu, X. T. Li, S. W. Zhang, X. T. Mi, and Y. G. Tang, "Ruling of echelles and gratings with a diamond tool by the torque equilibrium method," Appl. Opt. **55**, 8082–8088 (2016).
20. X. Pei, Y. Y. Li, and Z. X. Hou, "Performance measurement and experiment for rotational flexural joint with large-stroke," Opt. Precis. Eng. **21**, 927–933 (2013).
21. C. X. Wei, H. D. Chen, and D. Y. Yin, "Spatial compliant micro-displacement magnifying mechanism based on cross-spring flexural pivot," Opt. Precis. Eng. **23**, 3168–3175 (2015).
22. Y. Altintas and M. Aleck, "Chatter stability of metal cutting and grinding," CIRP Ann. Manuf. Technol. **53**, 619–642 (2004).